In Vivo MR Determination of Water Diffusion Coefficients and Diffusion Anisotropy: Correlation with Structural Alteration in Gliomas of the Cerebral Hemispheres

James A. Brunberg, Thomas L. Chenevert, P. E. McKeever, Donald A. Ross, Larry R. Junck, Karin M. Muraszko, Robert Dauser, James G. Pipe, and A. T. Betley

PURPOSE: To determine whether a relationship exists between water diffusion coefficients or diffusion anisotropy and MR-defined regions of normal or abnormal brain parenchyma in patients with cerebral gliomas. **METHODS:** In 40 patients with cerebral gliomas, diffusion was characterized in a single column of interest using a motion-insensitive spin-echo sequence that was applied sequentially at two gradient strength settings in three orthogonal directions. Apparent diffusion coefficients (ADCs) were derived for the three orthogonal axes at 128 points along the column. An average ADC and an index of diffusion anisotropy (IDA = diffusion coefficient$_{max\text{-}min}$/diffusion$_{mean}$) was then calculated for any of nine MR-determined regions of interest within the tumor or adjacent parenchyma. **RESULTS:** In cerebral edema, mean ADC (all ADCs as 10^{-7} cm^2/s) was 138 ± 24 (versus 83 ± 6 for normal white matter) with mean IDA of 0.26 ± 0.14 (versus 0.45 ± 0.17 for normal white matter). Solid enhancing central tumor mean ADC was 131 ± 25 with mean IDA of 0.15 ± 0.10. Solid enhancing tumor margin mean ADC was 131 ± 25, with IDA of 0.25 ± 0.20. Cyst or necrosis mean ADC was 235 ± 35 with IDA of 0.07 ± 0.04. **CONCLUSION:** In cerebral gliomas ADC and IDA determinations provide information not available from routine MR imaging. ADC and IDA determinations allow distinction between normal white matter, areas of necrosis or cyst formation, regions of edema, and solid enhancing tumor. ADCs can be quickly and reliably characterized within a motion-insensitive column of interest with standard MR hardware.

Index terms: Glioma; Brain neoplasms, magnetic resonance; Magnetic resonance, diffusion-weighted scanning; Magnetic resonance, tissue characterization

AJNR Am J Neuroradiol 16:361–371, February 1995

Tissue water diffusion is an intracellular and extracellular phenomenon. The magnitude and directional preponderance of diffusion is variably restricted by cell membranes and tissue macromolecules (1). The clinical importance of diffusion characterization in the central nervous system is that the magnitude and direction of this tissue property can be used to reflect normal or developmental tissue properties and to characterize gross and microscopic structural alterations associated with tissue disease. Although derived with magnetic resonance (MR) techniques, diffusion phenomena are largely separate from the T1 and T2 relaxation properties characterized by routine MR imaging. Initial studies in human subjects have demonstrated the utility of characterizing the apparent diffusion coefficient (ADC) of water in tissue for the evaluation of early stroke (2–5), for the demonstration of normal white matter fiber orientation as diffusion anisotropy (6–11), for the evaluation of intracranial tumors (12–15), and for the characterization of white matter lesions in both multiple sclerosis (14, 16) and pseudotumor cerebri (4, 17).

Techniques for the quantitative MR characterization of tissue water ADCs as incoherent

Received February 2, 1994; accepted after revision June 15.

This work was supported in part by a grant from General Electric Medical Systems.

From the Departments of Radiology (J.A.B., T.L.C., J.G.P., A.T.B.), Neurology (J.A.B., L.R.J.), Neurosurgery (J.A.B., D.A.R., K.M.M., R.D.), and Pathology (P.E.M.), University of Michigan Hospitals, Ann Arbor.

Address reprint requests to James A. Brunberg, MD, Department of Radiology, B2B 311, Box 0030, University of Michigan Medical Center, Ann Arbor, MI 48109-0030.

AJNR 16:361–371, Feb 1995 0195-6108/95/1602–0361

Fig 1. Pulse sequence diagram. Echo time is 125 milliseconds; δ, 36 milliseconds, Δ, 65.6 milliseconds, and A, 0.4 and 0.9 G/cm. Six gradient conditions (b1, b2) $\times$ (X, Y, Z) were collected iteratively and processed independently. *Shaded* sequence components, used to produce the pilot image, were off during the interleaved diffusion-sensitized portions.

intravoxel displacement over time and for the construction of diffusion-weighted images have been described (4, 8, 11–15, 18–24). Two factors have limited extensive clinical use of such characterization as an adjunct to MR imaging. The first has been the sensitivity of diffusion-weighted MR images and of quantitative determinations of ADCs to involuntary and physiologic patient movement (13, 21, 22, 24, 25). Such movement is associated with the production of phase-related artifact or with compromised voxel registration, either of which interferes with accurate ADC characterization. The second factor has been the expense and relative unavailability of MR gradient hardware necessary for echo-planar sequences, which, because of rapid image acquisition, are relatively motion insensitive.

In response to these technical limitations a motion-insensitive pulse sequence that uses standard MR hardware has been developed at our institution for the rapid quantitative determination of water ADCs in three orthogonal directions (6, 25). The purpose of this study was to determine whether water ADCs derived with a modified version of this sequence could provide useful information supplemental to that obtained from routine MR imaging in patients with cerebral gliomas. We wished to determine whether a correlation exists between MR-located regions of structurally normal or abnormal brain parenchyma and quantitative determinations of water ADCs and diffusion anisotropy, and to determine whether these techniques would allow distinction between tissue types not otherwise evident on MR imaging.

Materials and Methods

In vivo quantitative determinations of water ADCs were obtained on 40 patients with supratentorial gliomas of varying grade and type, as follows.

Astrocytoma II	6
Astrocytoma III	9
Glioblastoma	15
Giant cell astrocytoma	3
Oligodendroglioma II	3
Pilocytic astrocytoma	1
Ganglioglioma	3

Patients were from two to 74 years of age. No patients had clinical or routine MR evidence of neurologic disorders other than the primary neoplasms. Tumor diagnosis was established in all cases by stereotactic or excisional biopsy. Use of the pulse sequence for ADC characterization was approved by our institutional review board, and informed patient or parental consent was obtained.

MR imaging and ADC characterization were accomplished with a 1.5-T system with standard clinical gradient coil strength (1.0 G/cm) and a transmit-receive quadrature head coil. No head immobilization device was used. ADC was routinely characterized after the completion of routine clinical imaging including the administration of gadopentetate dimeglumine. Preliminary studies at this institution (unpublished) have demonstrated no alteration in ADC values in normal tissue or in abnormally enhancing tissue after contrast administration.

ADCs were determined in at least one 8-mm $\times$ 8-mm $\times$ 20-cm columnar region of interest. This column was located on the basis of coordinates derived from the MR image series. The pulse sequence used for ADC characterization was a modified Stejskal-Tanner spin-echo sequence at 1500/125 (repetition time/echo time) (Fig 1). The column of interest was established by the orthogonal placement of the planes of the 90° and 180° pulses of the pulse sequence so that only tissue at the intersection of these planes was interrogated for diffusion characterization. Two diffusion-gradient amplitudes (0.4 and 0.9 G/cm) were applied iteratively in three orthogonal directions for each column of interest, using timing as indicated in Figure 1. Gradient b factors were numerically calculated independently for each of the three orthogonal gradient wave forms; nominal b factors were 7940 and 40 140 s/cm^2.

Cardiac or peripheral gating was not used. Such gating would have lengthened each study and induced possible

Fig 2. Twenty-year-old patient with grade III astrocytoma.

A, Diffusion sequence pilot image.

T1-weighted images before (*B*) and after (*C*) gadopentetate dimeglumine administration demonstrate a well-demarcated nonenhancing lesion, which is bright on T2-weighted images (*D*).

E, Graph of diffusion characterization. The x-axis corresponds to the right-left positioning of the column of interest in the pilot image and to the column of interest superimposed on routine MR images. Diffusion results in the three diffusion directions are coded as a *solid, broken,* and *heavy broken lines*. In this patient the *open arrows* define the solid astrocytoma. The calculated tumor mean ADC was 176 $\times 10^{-7}$ cm^2/s and the mean IDA was 0.06. In normal deep frontal white matter (*solid closed arrows*) mean ADC was 77 $\times 10^{-7}$ cm^2/s and mean IDA 0.66. The *broken closed arrows* identify cerebrospinal fluid and cortex partial volume effect at the lateral surfaces of the brain.

error from variable impulse time. Column location and phase-insensitive averaging were designed specifically not to include a phase-encoding gradient and thereby to reduce pulsatility phase shift so that cardiac gating was not necessary. Variable T1 saturation effects during the initial pulses were avoided by excluding the first six diffusion-sensitizing echoes from data averaging.

Gradient wave forms were designed to minimize cross-terms in b factors. Cross-terms are contributions to diffusion sensitization that are induced by interactions between gradient pulses, which are applied specifically for a given directional diffusion characterization, and other gradient pulses, which are applied in the same direction for section selection or frequency encoding. Interaction between perpendicular gradient pulses can similarly affect diffusion sensitivity. In this study, gradient wave forms were designed to minimize these cross-terms and interactions between gradients. This was done by applying diffusion-sensitizing gradient pulses independently along the three orthogonal directions. It was also done by having the 90° radio frequency pulse and the frequency-encoding wave forms temporally integrated to zero when diffusion pulses

TABLE 1. ADC and IDA for each region of interest

Tissue of Interest	IDA					ADC				
	n	Mean	SD	Max	Min	n	Mean	SD	Max	Min
Nonenhancing solid tumor	18	143	33	199	81	18	0.16	0.12	0.48	0.04
Nonenhancing solid tumor, adjacent enhancement	5	128	24	172	103	5	0.15	0.04	0.22	0.10
Enhancing solid tumor	13	131	23	175	89	13	0.15	0.10	0.42	0.04
Enhancing tumor margin	26	131	25	191	101	26	0.24	0.15	0.73	0.08
Cyst or necrosis	24	235	35	274	141	22	0.07	0.04	0.15	0.02
Cyst confirmed at surgery	9	266	9	274	244	7	0.06	0.03	0.09	0.02
Edema	26	138	24	183	100	26	0.26	0.14	0.66	0.07
Normal-appearing adjacent white matter	8	80	8	95	70	8	0.70	0.20	1.00	0.35
Normal white matter	40	83	6	98	71	40	0.45	0.17	0.78	0.18
Normal cortical gray matter	15	90	4	97	83	15	0.19	0.06	0.30	0.10

were applied (Fig 1). The orthogonal 180° gradient pulse did contribute a cross-term, but its effect was negligible because the gradient pulse was short in duration.

Data from like gradient conditions were combined "in magnitude" to improve signal-to-noise ratio without risk of phase cancellation from gross motion phase shifts. At least 20 single excitations were combined for each diffusion gradient condition to improve signal-to-noise ratio and to reduce the random error in ADC values to approximately 10%. Each excitation represented a single incorporation of the pulse sequence (Fig 1), because phase-encoding steps were not used. A pilot image (Fig 2A) was interleaved with the diffusion data acquisition to assure proper positioning of the column of interest and to assure that there was no gross motion during the acquisition of diffusion data. Because the pilot image was interleaved with the ADC characterizing sequence, the prescribed column of interest was annotated on the image as a band of saturation. The entire acquisition time for three orthogonal directional ADC characterizations and for derivation of the pilot image was 6.5 minutes.

Time-domain data were transferred to a SPARC10 work station (Sun Microsystems, Mountain View, Calif) for processing with Advanced Visual Systems software (AVS, Waltham, Mass). Echoes were individually Fourier transformed. Quantitative accuracy of the sequence was determined to be within 5% using water and acetone phantoms. Frequency encoding along the 20-cm length of the column (128 steps) provided a resolution of 1.56 mm. Low bandwidth reception (8 kHz) was used to enhance the signal-to-noise ratio.

ADC values were calculated for each of the three axes of the column of interest ($ADC_{A\text{-}P}$, $ADC_{R\text{-}L}$, and $ADC_{S\text{-}I}$) using signal intensity (Sb1 and Sb2) at each of 128 segments along the length of the column of interest as:

$$1) \qquad ADC_i = \ln(Sb1_i/Sb2_i)(b2-bl_i)$$

where i is R-L, A-P, and S-I, and b1 and b2 are the two diffusion gradient settings. The data for each direction were independently portrayed in graphic form (Fig 2E). From these data a mean ADC ($ADC_{mean} = ADC_{(R\text{-}L)+(A\text{-}P)+(S\text{-}I)}/3$) and an index of diffusion anisotropy ($IDA = ADC_{max-min}/ADC_{mean}$) were calculated on a pixel-by-pixel basis. These data were than summarized for each chosen region of interest. ADCs were expressed as 1×10^{-7} cm^2/s. ADC_{max} and ADC_{min} were the ADCs for the maximal and the minimal diffusion values in the three orthogonal directions for each voxel. ADC_{mean} was the mean ADC for each voxel or region of interest.

To correlate ADCs with anatomic regions of interest, both the margins of the column in which the ADC was characterized and a locating grid were superimposed on routine T2-weighted images and on T1-weighted images obtained before and after gadopentetate dimeglumine administration (0.1 mmol/kg) (Fig 2B). In this manner ADCs were located independently from the nine specific regions of interest, as follows.

1. Nonenhancing solid tumor, no adjacent enhancement
2. Nonenhancing solid tumor surrounded by enhancing tumor
3. Enhancing solid tumor without a central nonenhancing component
4. Enhancing margins of tumor surrounding nonenhancing tumor, cyst, or necrosis
5. Central cyst or necrosis
6. White matter edema distal to margins of enhancement
7. Normal-appearing white matter adjacent to mass effect
8. Normal white matter, opposite hemisphere
9. Normal gray matter, opposite hemisphere

Each region of interest was defined by MR characteristics on T2-weighted images and on T1-weighted images without and with gadopentetate dimeglumine administration. Histologic correlation was available only from the central portion of each tumor and from areas of cystic alteration or necrosis. Biopsies were not done on regions of edema and areas of normal tissue. Not all such areas could be identified in each patient. In some patients the same tissue type was sampled more than once, but always at a different location. Each region was sampled for its ADCs only if partial volume effects could be avoided. Values for ADC_{mean} and IDA_{mean} were compared for each of the nine MR located regions of interest using *P* values calculated from Student's two-tailed *t* tests for unpaired groups.

TABLE 2. Mean ADC comparisons: *P* values

	Nonenhancing Tumor Peripheral Enhancement	Solid Enhancement: No Central Nonenhancement	Enhanced Margin	Cyst vs Necrosis	White Matter Edema	Adjacent Normal White Matter	Normal Remote White Matter	Normal Remote Gray Matter
Nonenhancing solid tumor, no adjacent enhancement	<.07	NS	NS	<.001	0.09	<.001	<.001	<.001
Nonenhancing solid tumor, peripheral enhancement	. . .	NS	NS	<.001	0.09	<.001	<.001	<.001
Solid enhancing tumor	NS	. . .	NS	<.001	NS	<.001	<.001	<.001
Enhancing tumor margin	NS	NS	. . .	<.001	NS	<.001	<.001	<.001
Cyst vs necrosis	<.001	<.001	<.001	. . .	<.001	<.001	<.001	<.001
White matter edema	<.001	NS	NS	<.001	. . .	<.001	<.001	<.001
Adjacent normal white matter	<.001	<.001	<.001	<.001	<.001	. . .	<.05	<.001
Normal remote white matter	<.001	<.001	<.001	<.001	<.001	<.05	. . .	<.001

Note.—NS indicates not significant ($P > .10$).

Results

Statistical data regarding mean ADC coefficients and calculated index of diffusion ansiotropy (IDA) for each of the nine regions of interest are listed in Table 1. ADC and IDA determinations were not significantly related to histologic type or grade for the nine selected regions of interest (data not shown). There were, however, statistically significant differences in mean ADCs and in IDAs between several of the nine regions of interest (Tables 2 and 3).

Three patients demonstrated mass lesions characterized by MR imaging as sharply demarcated solitary regions of unenhancing low signal intensity on T1-weighted images and as regions of high signal intensity on T2-weighted images (Fig 2). It was not possible in these patients to determine from MR imaging whether the lesions were cystic or solid. ADC characterization in each instance showed mean ADCs of 164, 199, and 109 $\times 10^{-7}$ cm^2/s. At surgery each of the lesions was demonstrated to be solid and firm.

In 18 patients MR imaging demonstrated alterations consistent with one or more regions of necrosis or cyst formation (Table 1). In 8 of these 18 patients stereotactic or open biopsies demonstrated at least one large distinct fluid collection (Fig 3). In 1 patient there was surgical confirmation of the presence of tumor necrosis unassociated with fluid collection (Fig 4). In this patient the mean ADC was 204 $\pm$ 14 $\times 10^{-7}$ cm^2/s, and the IDA was 0.14 $\pm$ 0.01. In the remaining 9 patients histologic findings or clinical appearance indicated the presence of small cysts intermixed with necrosis. None of these 18 patients were separated from the larger group designated as "cyst versus necrosis" on the basis of MR findings alone.

TABLE 3. Mean diffusion anisotropy comparisons: *P* values

	Nonenhancing Tumor Peripheral Enhancement	Solid Enhancing: No Central Nonenhancement	Enhanced Margin	Cyst vs Necrosis	White Matter Edema	Adjacent Normal White Matter	Normal Remote White Matter	Normal Remote Gray Matter
Nonenhancing solid tumor, no adjacent enhancement	NS	NS	0.08	<.001	<.02	<.001	<.001	NS
Nonenhancing solid tumor, peripheral enhancement	. . .	NS	0.09	<.001	<.001	<.001	<.001	<.07
Solid enhancing tumor:	NS	. . .	<.05	<.001	<.001	<.001	<.001	NS
Enhancing tumor margin	<.09	<.05	. . .	<.001	NS	<.001	<.001	NS
Cyst vs necrosis	<.001	<.001	<.001	. . .	<.001	<.001	<.001	<.001
White matter edema	<.001	<.001	NS	<.001	. . .	<.001	<.001	<.05
Adjacent normal white matter	<.001	<.001	<.001	<.001	<.001	. . .	<.001	<.001
Normal remote white matter	<.001	<.001	<.001	<.001	<.001	<.001	. . .	<.001

Note.—NS indicates not significant ($P > .10$).

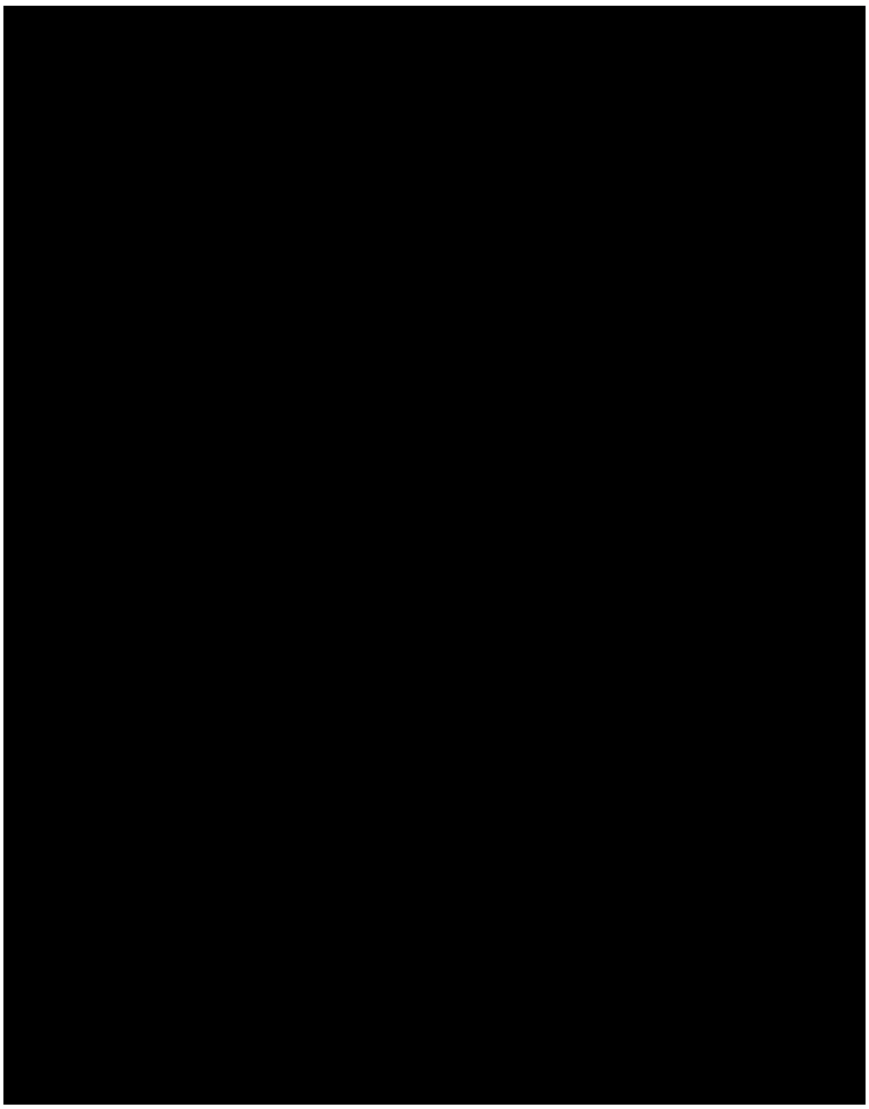

Fig 3. Thirty-eight-year-old patient with glioblastoma.

A, T1-weighted image after gadopentetate dimeglumine administration demonstrates mass with contrast-enhancing margins and two separate nonenhancing regions of differing signal intensity.

B, On T2-weighted images two areas of central high signal intensity are identified.

C, The diffusion graph demonstrates two areas (*closed broken* and *closed solid arrows*) in which mean diffusion coefficients were 246 and 244 $\times$ 10^{-7} cm^2/s. Cystic fluid was drained from each area at surgery. In the region of apparent frontal edema (*open arrows*) mean ADC was 179 $\times$ 10^{-7} cm^2/s with a mean IDA 0.21.

Discussion

Techniques for the MR characterization and display of tissue water diffusion, both as incoherent intravoxel displacement over time and as diffusion-weighted images, have been described (4, 8, 11, 18, 20, 21, 24). With each of these techniques the occurrence of intravoxel water-proton diffusion in the presence of a strong intravoxel magnetic gradient causes signal loss relative to what would be observed from nondiffusing protons. This signal alteration is caused by loss in phase coherence as diffusing protons of water move within the voxel, which has a steep imposed intravoxel magnetic gradient applied in positive and negative directions (Fig 1). Nondiffusing protons do not alter their net phase in response to this symmetric bidirectional gradient imposition. Ratios of intravoxel signal intensity derived from at least two independent sequences with gradients of differing but known strength can then be used to calculate quantitative ADCs (equation 1).

Tissue water diffusion is complex to characterize. Its magnitude and direction depend on the permeability and spacing of diffusion barriers, viscosity of the suspending medium, and duration of diffusion observation (1). Characterization is also complicated by bulk flow within capillaries and by tissue water active transport processes. Protons characterized in the brain are contained in water, whereas protons within macromolecules and membranes themselves make no contribution to diffusion characterization because they are relatively immobile and

Fig 4. Fifty-three-year-old patient with glioblastoma.

Coronal T1-weighted images before (*A*) and after (*B*) contrast administration demonstrate a nonenhancing central region, which is high in signal intensity on the T2-weighted series (*C*).

D, The diffusion graph demonstrates an area of varying diffusion (*between open arrows*) with mean diffusion of 204 $\times$ 10^{-7} cm^2/s and mean IDA of 0.14. At surgery this tissue was predominately necrotic but firm tumor. There was no fluid component. The enhancing tumor capsule (*between closed solid arrows*) had a mean diffusion of 153 with a mean IDA of 0.08. The region between the *closed broken arrows* represents partial volume effect of ventricular cerebrospinal fluid.

have extremely short T2 values. Although cellular membranes are permeable to water, the movement of water molecules through such membranes is restricted. To express diffusion anisotropy as a single value within a voxel or region of interest we used the calculated relationship IDA = $ADC_{max\text{-}min}/ADC_{mean}$ (see "Materials and Methods"). The mean IDA in regions of interest varied from 0.06 in regions of cyst confirmed at surgery, in which there would be no internal structural diffusion barriers, to 0.70 in normal appearing white matter immediately adjacent to an area of mass effect, in which internal preservation of white matter myelin orientation would be preserved (Table 1).

Diffusion data reported in this study have been characterized as ADCs, which were derived in each of three orthogonal directions. From these data a mean ADC and an IDA have been derived. It is recognized that diffusion in an anisotropic system is described as a tensor quantity that may be represented as a diffusion ellipsoid. The lengths and orientations of the principal axes of the ellipsoid include magnitude and direction of maximal and minimal diffusitivities. From these axes an expression of anisotropy may be derived. The IDA used in this study is analogous but is limited by the derivation of diffusion coefficients from the x-, y-, and z-axes of the scanner. The mean ADC determined in this study is proportional to the trace of the diffusion tensor, which as a scaler invariant of the tensor is not limited by the three-directional measurement scheme of this study.

Although water-diffusion phenomena are quantified by MR techniques, and MR relaxation rates have diffusion dependencies, diffusion is largely separate from T1 and T2 properties that determine contrast in conventional MR imaging. Characterization of diffusion is not a significant component of routine MR imaging. The quanti-

fication of ADCs relies instead on the characterization of intravoxel alteration in signal intensity in response to imposed bipolar gradients as described above. The independence of T1 and T2 properties from ADC characterization is illustrated by the occurrence of high signal on T2 images within lesions that do not enhance after gadopentetate dimeglumide administration and that by ADC characterization and surgical observation may be solid (Fig 2) or cystic (Fig 3).

Phase-related artifact from patient movement and from physiologic brain pulsation has limited the utility of ADC characterization with routine imaging hardware. In the current study the elimination of phase-encoding localization and the use of phase-insensitive processing permitted the acquisition of a one-dimensional image that could be used for ADC characterization in a specific region of interest. Phase-insensitive processing eliminated nearly all motion artifact that originates from bulk motion phase shifts. The incorporation of this column technique as a probe for the characterization of ADCs within a region of interest has provided rapid and reproducible data that are relatively free of artifact without the use of head-immobilization devices. The absence of a diffusion "image" has not prevented the incorporation of ADC data into clinical patient treatment.

Published data regarding the characterization of ADCs in the intracranial tumors are limited. Low qualitative diffusion in epidermoids relative to cerebrospinal fluid has been recognized (13). Quantitative characterization of ADCs in a patient with cerebral astrocytomas has indicated an ADC of less than 150×10^{-7} cm^2/s (12). In a patient with oligodendroglioma ADC, values were less than 190 to 200×10^{-7} cm^2/s (26). In a review of imaging of anisotropically restricted diffusion of water in the nervous system, Hajnal et al (14) made reference to additional unreported patients who had glioma with elevated qualitative ADCs within tumor tissue and to elevated quantitative ADCs in surrounding edema (179 and $249 \times 10^{-7} cm^2/s$) and regions of tumor necrosis ($238 \times 10^{-7} cm^2/s$) or cyst ($257$ and $265 \times 10^{-7} cm^2/s$) formation (14). These ADC determinations were all obtained with differing hardware, with varying pulse sequences, and with varying motion-suppressing techniques. In general, the findings have been within the range of the values demonstrated in the current study (Table 1).

In the current series of 40 patients with cerebral gliomas, statistically different mean values for quantitative ADCs and for calculated values of diffusion anisotropy were detected between MR-located regions of interest at the site of the tumor and normal gray and white matter of the opposite hemisphere. Normal white matter was consistently associated with diffusion anisotropy, as previously reported (6). This directional preponderance of diffusion most likely arises as the result of relative restriction of transverse diffusion by longitudinal myelinated fiber orientation. Because water diffusion in white matter is restricted (1), ADC values are in part determined by the relative orientation of the magnetic field gradient and the predominate direction within each voxel. This diffusion anisotropy provides information not otherwise available from MR imaging regarding relative myelin fiber orientation within each voxel and regarding the integrity and state of development of the myelin sheath. ADC values are lower perpendicular to the axis of the axon because the myelin sheath is less permeable to water then is the axonal cytoplasm, because water within myelin has a short T2 and is not characterized by the sequence used for ADC determination, and because the longitudinal configuration of the axonal cytoplasm promotes the diffusion or transport of water in a longitudinal rather than transverse direction.

White matter diffusion anisotropy in our series varied depending on the region of brain parenchyma sampled. The highest values for diffusion anisotropy were found in the corpus callosum, in the superior longitudinal fasiculus, and in the arcuate fasciculus. The lowest values were in white matter at the junction of longitudinal fasciculi with subcortical association fibers. Cerebral cortex, which is distinctly less myelinated than white matter, had a slightly higher mean ADC coefficient but distinctly lower diffusion anisotropy than did white matter (Fig 5). The mean values of ADCs and diffusion anisotropy for normal cortical gray matter and white matter differed from each other with statistical significance (Tables 2 and 3). Mean ADCs for cortical gray matter and for white matter were also statistically distinct from mean ADCs in all other sampled areas. The lack of a significant difference in mean diffusion anisotropy between gray matter and enhancing tumor margins, solid enhancing tumor, and nonenhancing solid tumor most likely reflects the

Fig 5. Eighteen-year-old patient with grade II astrocytoma.

Coronal T1-weighted images before (*A*) and after (*B*) contrast administration show a densely enhancing cortical lesion, which is high in signal on T2-weighted images (*C*). There is a region of apparent edema medial to the enhancing lesion (*C*).

D, The enhancing component of the lesion (*between closed broken arrows*) had a mean diffusion of 156×10^{-7} cm^2/s with an IDA of 0.06. The normal left temporal cortex (*between open arrows*) had a mean ADC of 87×10^{-7} cm^2/s with an IDA 0.14. In the region of apparent edema (*between closed solid arrows*) the mean ADC was $119 \times 10^{\times 7}$ cm^2/s with an IDA of 0.19. The presence or absence of tumor cells within this region of apparent edema was not histologically confirmed.

disruption of myelinated fiber orientation by the tumor process.

Adjacent to areas of mass effect, the presence of displaced and distorted white matter is frequently demonstrated with MR imaging. This white matter may be normal or low in signal intensity on T2-weighted images. In eight patients with displaced or distorted white matter, mean ADCs and diffusion anisotropy in these regions differed significantly from each of the other eight areas characterized. The slightly lower mean ADC values and higher diffusion anisotropy in these regions relative to normal white matter in the opposite hemisphere may relate to mechanical compression of myelin with diminished extracellular water content or may relate to relative ischemia from compression of the capillary bed. Previous studies have established the occurrence of diminished ADCs in the presence of ischemia, possibly because of the shift of water to a more intracellular environment in which diffusion is more restricted by intracellular organelles and macromolecules.

Regions of white matter edema distal to enhancing tumor margins demonstrated mean ADC values that were significantly different from normal remote cortical gray matter and white matter, from adjacent normal-appearing white matter, and from areas of tumor cyst or necrosis (Fig 3). There was no difference between ADCs derived from regions of edema and those derived from regions of enhancing or nonenhancing tumor. This lack of distinction most likely relates to increased intercellular water within edematous white matter and within tumor at the site of replacement of normal brain parenchyma. However, a significant difference in mean diffusion anisotropy was demonstrated between regions of white matter edema and regions of enhancing or nonenhancing tumor.

This difference in anisotropy most likely reflects the presence of intact myelin membranes within white matter edema and the loss of this diffusion-restricting boundary in areas of contiguous tumor cell proliferation.

In regions of cyst formation or necrosis there was diminished or absent diffusion anisotropy relative to other tissue types sampled, and ADC values were markedly elevated (Tables 1 and 2). Regions suspected to be cystic or necrotic on the basis of MR imaging could be reliably distinguished as a group from the eight other tissue types on the basis of either ADC characteristic ($P < .001$). Eight patients had large cysts, the fluid contents of which were confirmed at the time of surgery or biopsy. Four were in glioblastomas, and four were in other tumor types. ADCs for this subgroup had a narrow range of 244 to 274 $\times 10^{-7}$ cm^2/s with a mean of 266 $\times 10^{-7}$ cm^2/s and SD of 9 $\times 10^{-7}$ cm^2/s. Mean diffusion anisotropy was 0.06 with a range of 0.02 to 0.09 and an SD of 0.03. These findings are consistent with our previous findings of an absence of diffusion anisotropy in cystic lesions of origins other than tumor that involve the brain or spinal cord (unpublished data). With cystic lesions from causes other than tumor, ADCs may approach that of cerebrospinal fluid (300 $\times 10^{-7}$ cm^2/s), most likely because of lower concentration of protein or other macromolecules within such fluid. ADCs of low-molecular-weight solvents such as water are lowered by factors of two to the three times when added polymer concentrations reach 30% (1). Among patients with suspected cyst formation or regions of tumor necrosis a mean ADC of greater than 250 and a mean IDA of less than 0.05 has consistently been associated with the presence of fluid as demonstrated at surgery or with aspiration at the time of stereotactic biopsy.

The ability to distinguish cystic or necrotic areas from regions of solid or extremely viscous tissue before surgery is of significant clinical use in designing the surgical approach to a lesion. Routine MR imaging does not consistently distinguish cystic from solid gliotic nonenhancing alterations. ADC characterization is now routinely accomplished at this institution as a component of preoperative MR evaluation. The ability to distinguish tissue consistency with ADC characterization is also used in establishing the utility of percutaneous aspiration for the treatment of rapidly increasing intracranial pressure in patients with glioblastomas or cystic astrocytomas.

A significant difference between mean ADCs of nonenhancing and enhancing tumor tissue was not demonstrated. Evaluations of diffusion anisotropy did, however, indicate greater persistence of anisotropic diffusion in enhancing tumor margins than in central enhancing or nonenhancing tumor. This finding may relate to persisting structural organization at the enhancing tumor margin, possibly caused by persisting although abnormal myelinated white matter, as tumor spreads peripherally. The lower values for diffusion anisotropy in central, more-established regions of tumor growth may reflect the loss of native myelinated pathways and their influence on diffusion anistropy as the tumor matures. A difference in ADCs or diffusion anisotropy between glioma types or grades within each of the nine regions of interest was not demonstrated.

Although ADCs alone did not distinguish between enhancing central tumor and surrounding edema, there was a significant difference in diffusion anisotropy between these two regions. Higher diffusion anisotropy was also demonstrated at the enhancing margin of a tumor than in an enhancing central lesion. These findings may again be consistent with greater disruption of diffusion-restricting myelin membranes in the more established central tumor mass. Enhancing lesions localized to the cerebral cortex were noted to have lower diffusion anisotropy than lesions centered in deep white matter.

In conclusion, quantitative brain water ADCs can be rapidly characterized within a region of interest using a modified Stejskal-Tanner spin-echo pulse sequence, standard MR gradient hardware, and a quadrature head coil. The derivation of data from a column of interest by the methods described significantly suppresses artifact originating from bulk motion phase shifts. ADCs thereby derived provide information independent of T1 and T2 characterization and supplemental to routine MR imaging. The differentiation among cystic, necrotic, and solid lesions, not always evident on routine MR imaging, was reliably accomplished with this technique. Such differentiation can be critical for the design of surgical and radiation treatment planning in patients with cerebral gliomas. The characterization of ADCs and IDA in regions of interest surrounding cerebral gliomas correlates with known concepts of destruction or preservation

of myelinated pathways in regions of adjacent tumor necrosis, enhancement, and edema.

References

1. Tanner JE. Intracellular diffusion of water. *Arch Biochem Biophys* 1983;224:416–428
2. de Crespigny AJ, Tsuura M, Moseley ME, Kucharczyk J. Perfusion and diffusion MR imaging of thromboembolic stroke. *J Magn Reson Imaging* 1993;3:746–754
3. Warach S, Chien D, Li W, Ronthal M, Edelman RR. Fast magnetic resonance diffusion-weighted imaging of acute human stroke. *Neurology* 1992;42:1717–1723
4. Thomsen C, Henriksen O, Ring P. In vivo measurement of water self diffusion in the human brain by magnetic resonance imaging. *Acta Radiol* 1987;28:353–361
5. Chien D, Kwong KK, Gress DR, Buonanno FS, Buxton RB, Rosen BR. MR diffusion imaging of cerebral infarction in humans. *AJNR Am J Neuroradiol* 1992;13:1097–1102
6. Chenevert TL, Brunberg JA, Pipe JG. Anisotropic diffusion in human white matter: demonstration with MR techniques in vivo. *Radiology* 1990;177:401–405
7. Rutherford MA, Cowan FM, Manzur AY, et al. MR imaging of anisotropically restricted diffusion in the brain of neonates and infants. *J Comput Assist Tomogr* 1991;15:188–198
8. Chien D, Buxton RB, Kwong KK, Brady TJ, Rosen BR. MR diffusion imaging of the human brain. *J Comput Assist Tomogr* 1990; 14:514–520
9. Doran M, Hajnal JV, Van Bruggen N, King MD, Young IR, Bydder GM. Normal and abnormal white matter tracts shown by MR imaging using directional diffusion weighted sequences. *J Comput Assist Tomogr* 1990;14:865–873
10. Sakuma H, Nomura Y, Takeda K, et al. Adult and neonatal human brain: diffusional anisotropy and myelination with diffusion-weighted MR imaging. *Radiology* 1991;180:229–233
11. Douek P, Turner R, Pekar J, Patronas N, Le Bihan D. MR color mapping of myeling fiber orientation. *J Comput Assist Tomogr* 1991;15:923–929
12. Le Bihan D, Breton E, Lallemand D, Grenier P, Cabanis E, Laval-Jeantet M. MR imaging of intravoxel incoherent motions: application to diffusion and perfusion in neurologic disorders. *Radiology* 1986;161:401–407
13. Tsuruda JS, Chew WM, Moseley ME, Norman D. Diffusion-weighted MR imaging of the brain: value of differentiating between extraaxial cysts and epidermoid tumors. *AJNR Am J Neuroradiol* 1990;11:925–931
14. Hajnal JV, Doran M, Hall AS, et al. MR imaging of anisotropically restricted diffusion of water in the nervous system: technical, anatomic, and pathologic considerations. *J Comput Assist Tomogr* 1991;15:1–18
15. Le Bihan D, Breton E, Lallemand D, Aubin M-L, Vignaud J, Laval-Jeantet M. Separation of diffusion and perfusion in intravoxel incoherent motion MR imaging. *Radiology* 1988;168:497–505
16. Larsson HBW, Thomsen C, Frederiksen J, Stubgaard M, Henriksen O. In vivo magnetic resonance diffusion measurement in the brain of patients with multiple sclerosis. *Magn Reson Imaging* 1992;10:7–12
17. Sørensen PS, Thomsen C, Gjerris F, Henriksen O. Brain water accumulation in pseudotumour cerebri demonstrated by MR-imaging of brain water self-diffusion. *Acta Neurochir [Supp] (Wien)* 1990;51:363–365
18. Le Bihan D, Breton E, Lallemand D, Aubin M-L, Vignaud J, Laval-Jeantet M. Separation of diffusion and perfusion in intravoxel incoherent motion MR imaging. *Radiology*. 1988;168:497–505
19. Harada K, Fujita N, Sakurai K, Akai Y, Fujii K, Kozuka T. Diffusion Imaging of the human brain: a new pulse sequence application for a 1.5-T standard MR system. *AJNR Am J Neuroradiol* 1991;12: 1143–1148
20. Sotak CH, Li L. MR imaging of anisotropic and restricted diffusion by simultaneous use of spin and stimulated echoes. *Magn Reson Med* 1992;26:174–183
21. Prasad PV, Nalcioglu O. A modified pulse sequence for *in vivo* diffusion imaging with reduced motion artifacts. *Magn Reson Med* 1991;18:116–131
22. Turner R, Le Bihan D, Maier J, Vavrek R, Hedges LK, Pekar J. Echo-planar imaging of intravoxel incoherent motion. *Radiology* 1990;177:407–414
23. Moseley ME, Sevick R, Wendland MF, et al. Ultrafast magnetic resonance imaging: diffusion and perfusion. *Can Assoc Radiol J* 1991;42:31–38
24. Johnson GA, Maki JH. In vivo measurement of proton diffusion in the presence of coherent motion. *Invest Radiol* 1991;26:540–545
25. Chenevert TL, Pipe JG, Williams DM, Brunberg JA. Quantitative measurement of tissue perfusion and diffusion *in vivo*. *Magn Reson Med* 1991;17:197–212
26. Hajnal JV, Doran M, Hall AS, et al. MR imaging of anisotropically restricted diffusion of water in the nervous system: technical, anatomic, and pathologic considerations. *J Comput Assist Tomogr* 1991;15:1–18

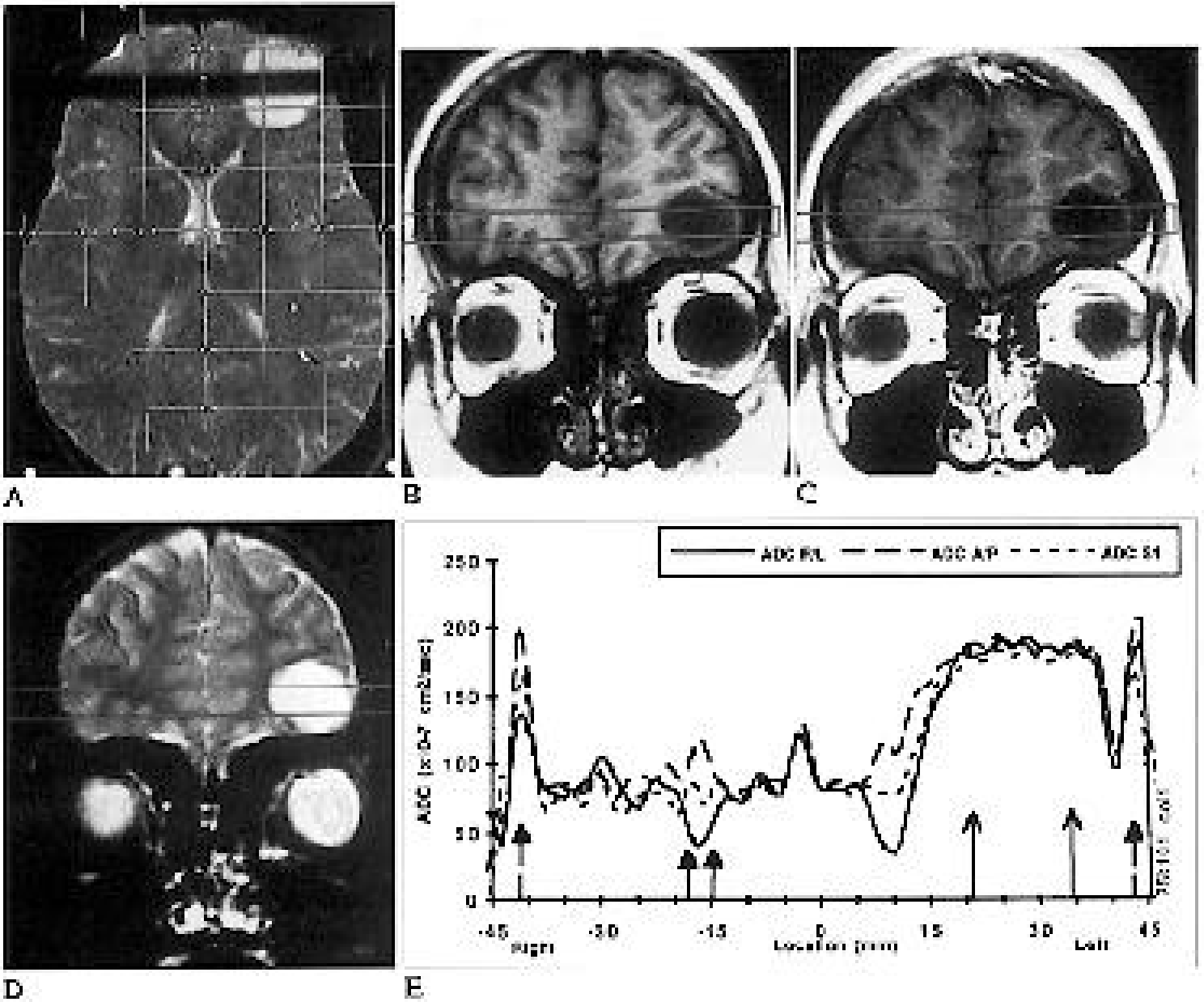
A
B
C
D
E
ADC RL
ADC AP
ADC SI
250
200
150
100
50
0
-45
-30
-15
0
15
30
45
Right
Location (mm)
Left

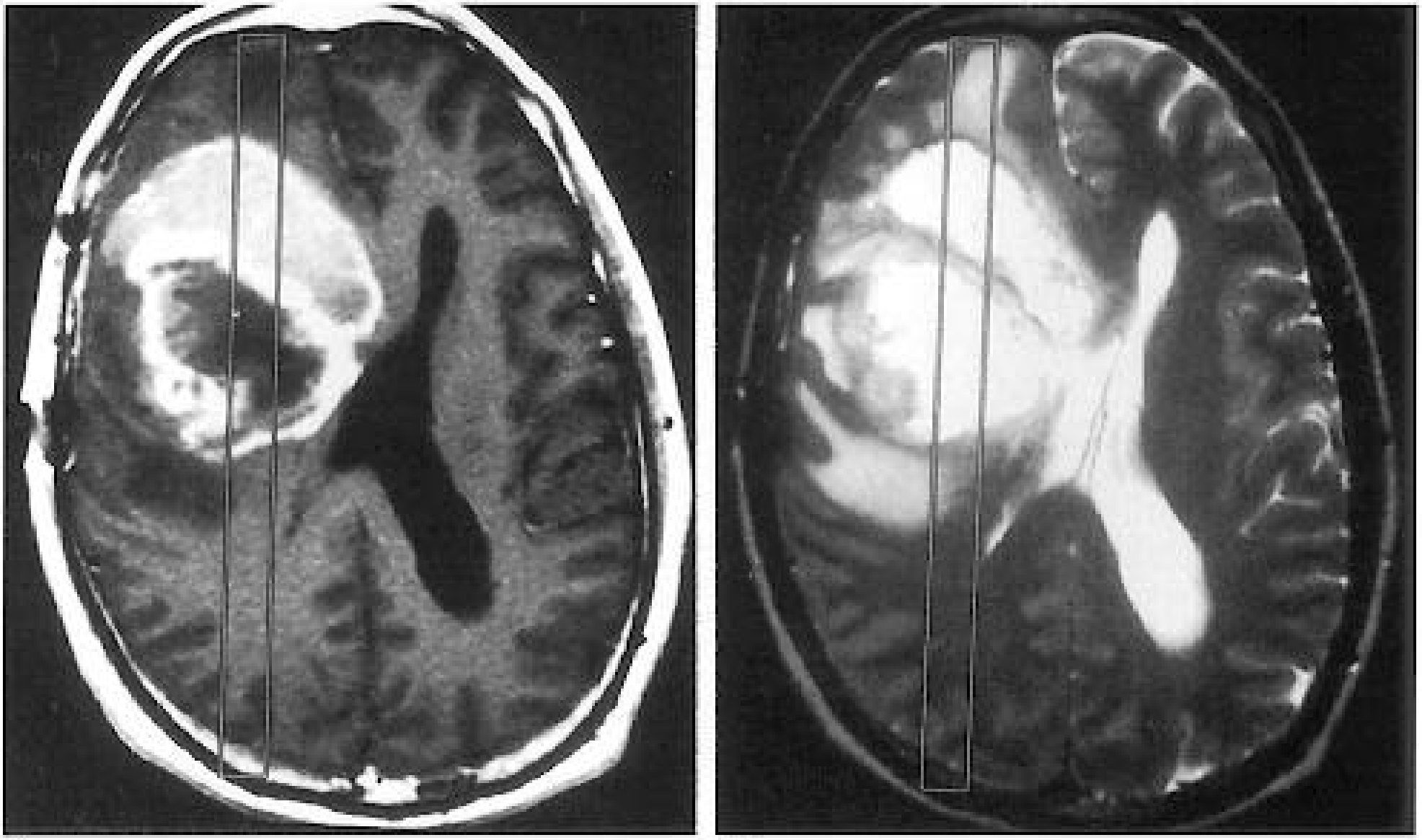
A
B

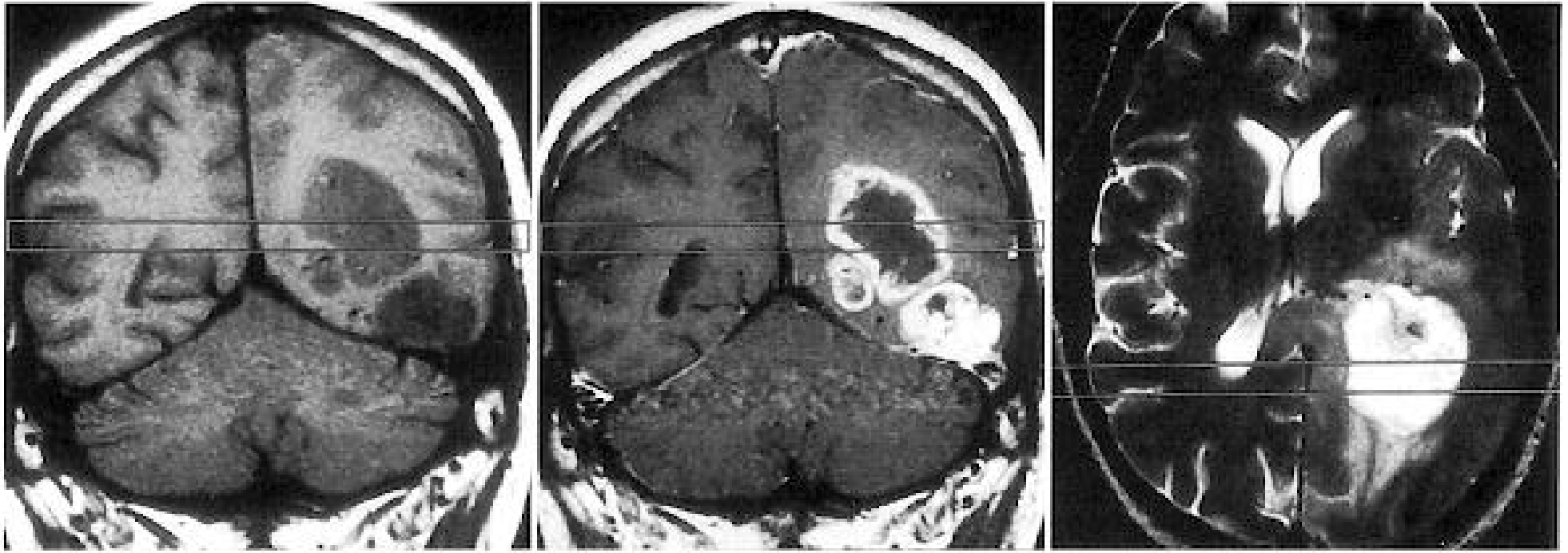
A
B
C

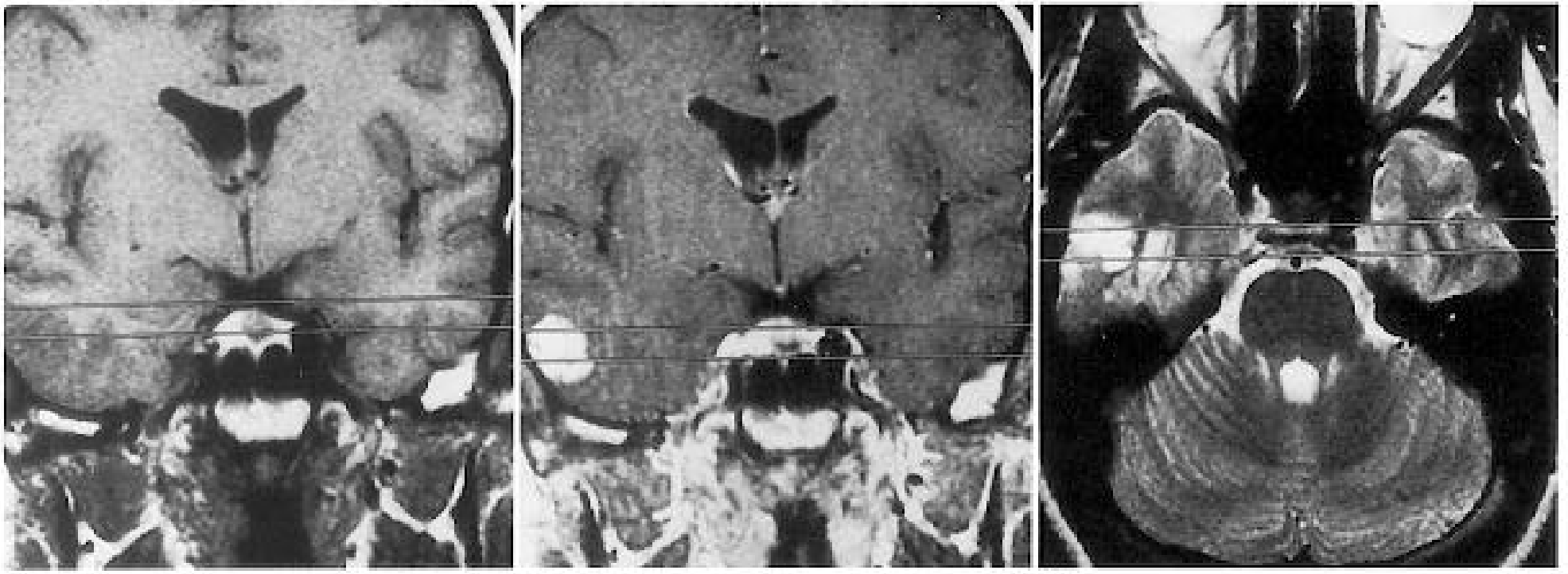
A
B
C

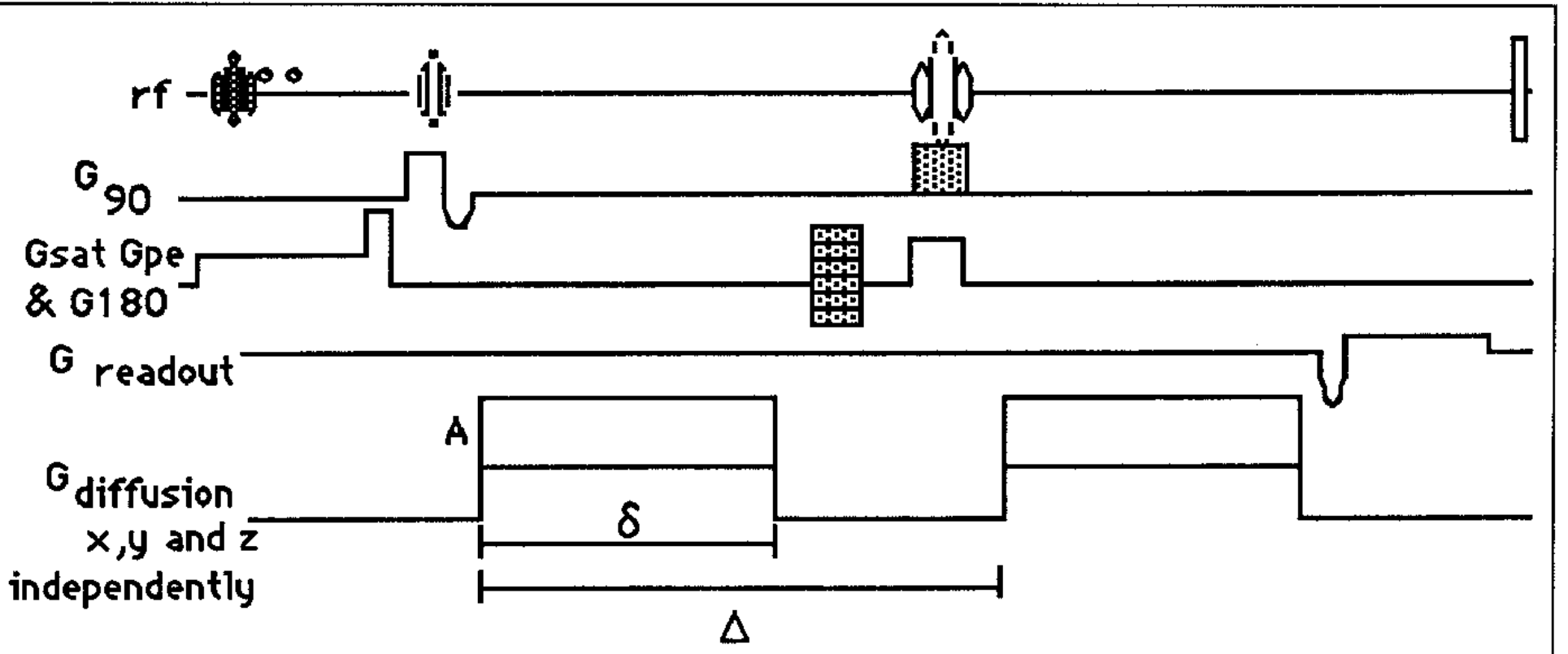
rf
G 90
Gsat Gpe
& G180
G readout
A
G diffusion
x,y and z
independently
δ
Δ

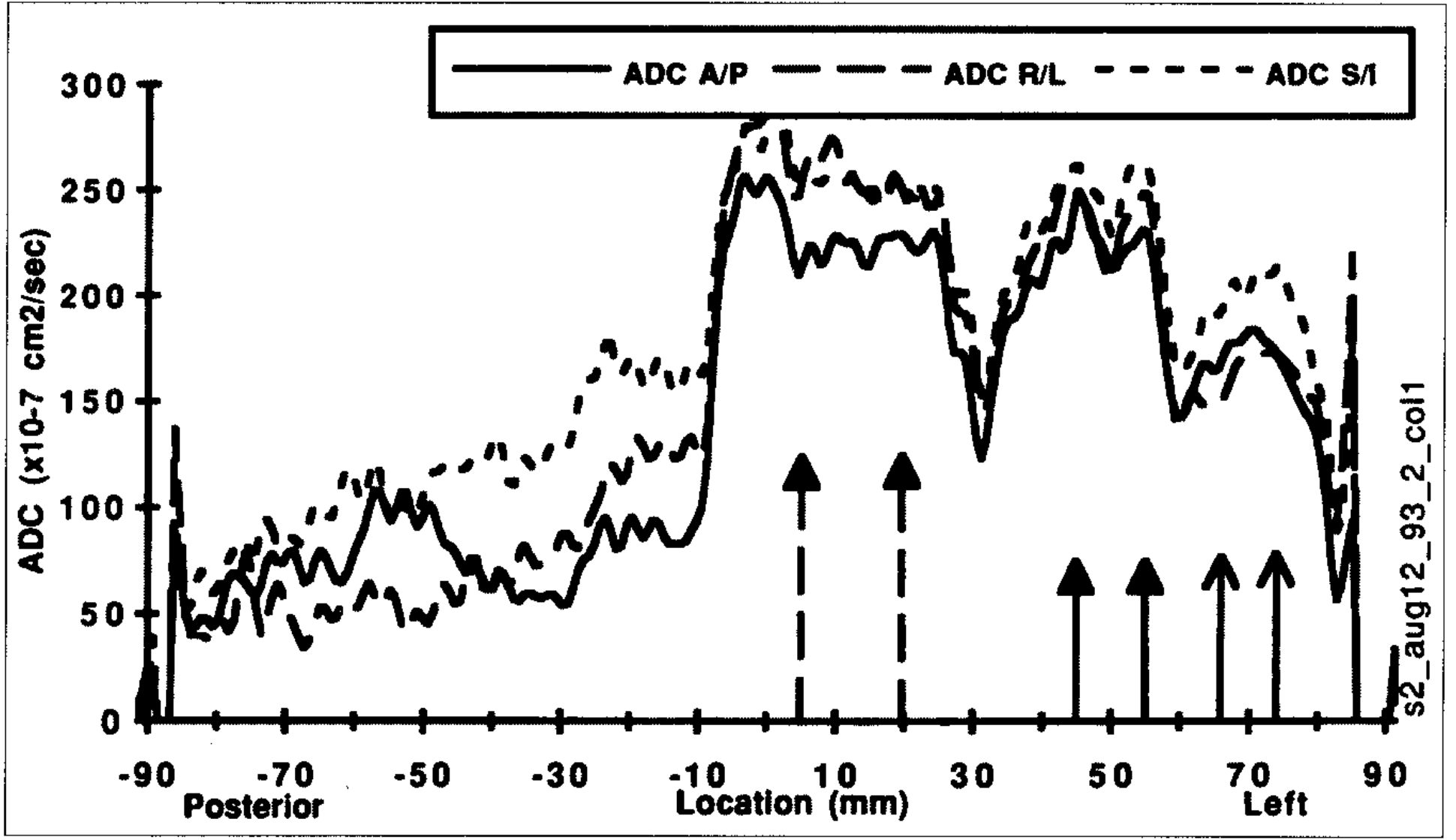
ADC A/P
ADC R/L
ADC S/I
300
250
200
150
100
50
0
ADC (x10-7 cm2/sec)
-90
-70
-50
-30
-10
10
30
50
70
90
Posterior
Location (mm)
Left
s2_aug12_93_2_col1

C

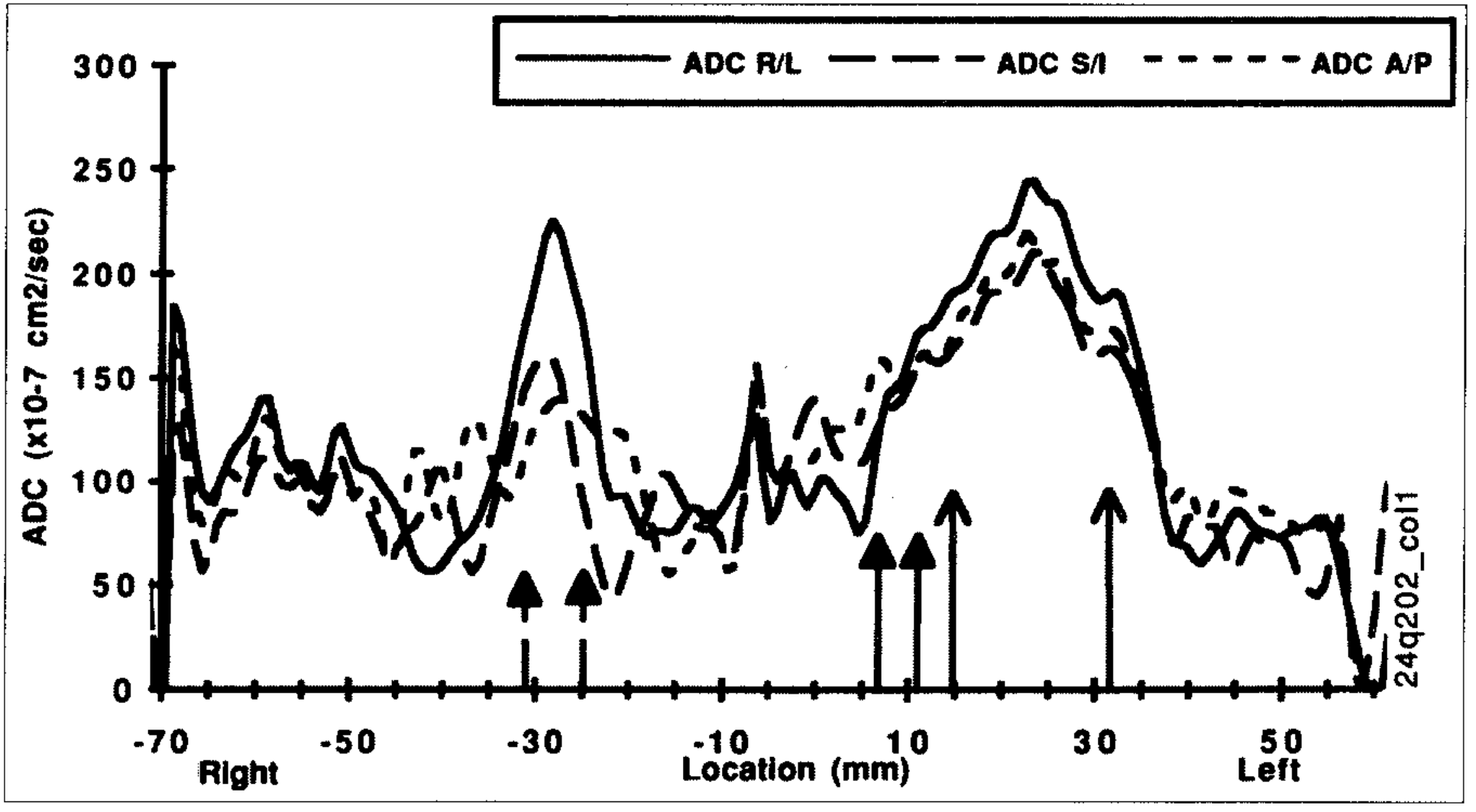
ADC R/L
ADC S/I
ADC A/P
300
250
200
150
100
50
0
ADC (x10-7 cm2/sec)
-70
-50
-30
-10
10
30
50
Right
Location (mm)
Left
24q202_col1

D

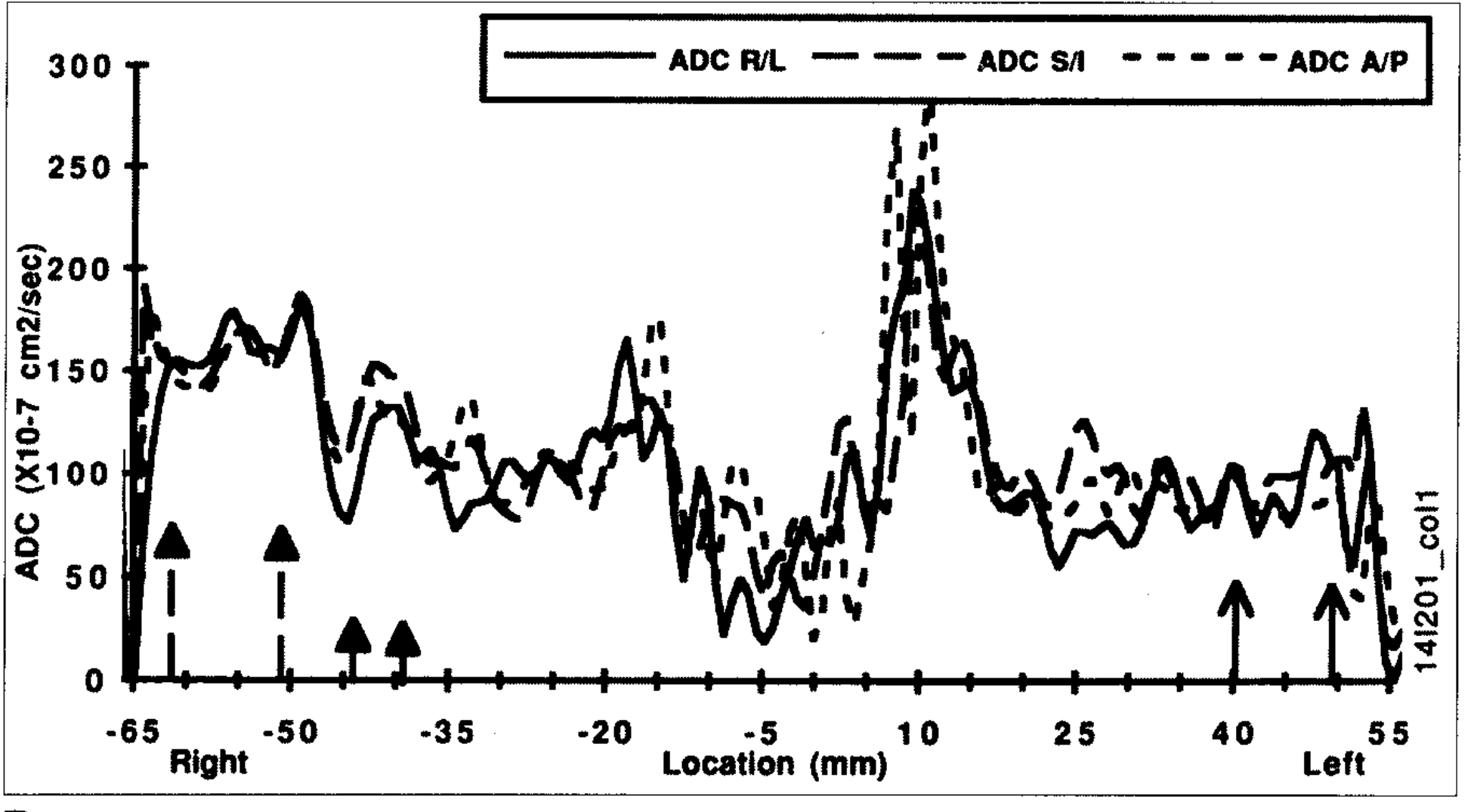
ADC R/L
ADC S/I
ADC A/P
300
250
200
150
100
50
0
ADC (X10-7 cm2/sec)
-65
-50
-35
-20
-5
10
25
40
55
Right
Location (mm)
Left
14I201_col1

D